THE JOURNAL OF PHYSICAL CHEMISTRY C

ARTICLE

pubs.acs.org/JPCC

Surface Morphologies of Size-Selected $Mo_{100\pm2.5}$ and $(MoO_3)_{67\pm1.5}$ Clusters Soft-Landed onto HOPG

K. A. Wepasnick, X. Li, T. Mangler,[†] S. Noessner,[†] C. Wolke,[†] M. Grossmann,[†] G. Gantefoer,*[,†] D. H. Fairbrother,* and K. H. Bowen*

Departments of Chemistry and Materials Science, Johns Hopkins University, Baltimore, Maryland 21218, United States

ABSTRACT: Mass-selected, cluster anion beams of $Mo_{100\pm2.5}^-$ and $(MoO_3)_{67\pm1.5}^-$ were prepared with a magnetron source and soft-landed onto highly ordered pyrolytic graphite (HOPG) under UHV conditions. These two clusters were selected because they possess essentially the same masses and consequently could be soft-landed with the same low kinetic energies. The chemical composition of the deposited clusters was analyzed using *in situ* Auger electron spectroscopy and *ex situ* X-ray photoelectron spectroscopy, while their surface morphologies were characterized with *in situ* scanning tunneling microscopy (STM) and *ex situ* atomic force microscopy (AFM). Both STM and AFM results indicated a high mobility for the metal atom clusters on HOPG at room temperature. At low coverages, $Mo_{100\pm2.5}$ clusters nucleated preferentially at step-edges. As their coverage increased, cluster aggregates formed on the terraces until a fully saturated overlayer was created. By contrast, deposited metal oxide clusters produced a stochastic array of adsorbed clusters for all coverages. Differences in the behavior of deposited $Mo_{100\pm2.5}$ and $(MoO_3)_{67\pm1.5}$ clusters were interpreted in terms of differences in the interactions of metal and metal oxide clusters with carbonaceous substrates.

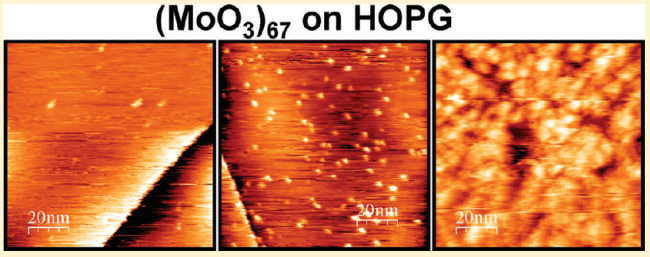

INTRODUCTION

Small, gas-phase (free) clusters often exhibit extraordinarily novel electronic, magnetic, and catalytic properties compared to bulk materials having the same compositions.[1−15] Such properties are strongly dependent on cluster size, even to the point where the addition or removal of a single atom can vastly alter a given property. To harness their finite-size properties for potential applications in the macroscopic world, however, most clusters will either have to reside on surfaces or be incorporated into materials.[16] In the former case, clusters would exist as ultrathin films, while in the latter case, clusters would be present in three-dimensional, "cluster assembled materials" either as guests embedded in inert hosts or as chemically bound surrogates for atoms within an otherwise traditional crystal lattice. In a few cases, species generated in cluster-forming environments are individually stable and can form macroscopic materials by themselves (e.g., fullerenes). Most clusters, however, require a hospitable medium to avoid agglomeration and thus retain their unique finite-size properties. For this reason, it is important to understand how clusters interact with each other and the surrounding environment.

In this paper, we focus on size-selected clusters residing on surfaces. Many studies have been conducted in which clusters were grown on surfaces by physical vapor deposition; these methods usually result in wide distributions of cluster sizes.[17−22] However, given that the unique properties of small clusters are strong functions of their sizes, better control can be achieved by depositing size-selected clusters onto surfaces. Indeed, the deposition of size-selected clusters onto surfaces has been an attractive topic of research for over a decade now;[23−90] a caveat to size-selection is that it requires that the clusters be charged so they can be separated based on their mass-to-charge ratio by mass spectrometry.

In a typical size-selected cluster experiment, cluster ions are produced in an appropriate ion source and transported in vacuum, as an ion beam, through a mass selector prior to being decelerated and deposited onto a target surface. This technique is capable of depositing clusters onto a substrate with well-defined sizes and landing energies. Furthermore, the deposition energy of the cluster ions can be tuned to low kinetic energies (soft-landing) to minimize damage to both the deposited cluster and the target surface, while cluster coverage on the substrate can be controlled by adjusting cluster ion intensities or deposition times.

Highly ordered pyrolytic graphite (HOPG) surfaces are often employed as substrates because their surfaces are atomically smooth, chemically inert, and easy to prepare.[69−101] Most earlier studies which utilized HOPG surfaces focused on depositing metal clusters, either by soft-landing or "pinning". Pinning involves depositing cluster ions at relatively high kinetics energies, so that they become stuck (pinned) upon deposition. Typically, pinned clusters are immobile on the surface, unless they are annealed at high temperature where they can become mobile.[70] By contrast, soft-landed metal clusters on HOPG at room temperature are mobile and tend to diffuse until they are

Received: March 7, 2011
Revised: April 22, 2011

   dx.doi.org/10.1021/jp202165u | *J. Phys. Chem. C* XXXX, XXX, 000–000

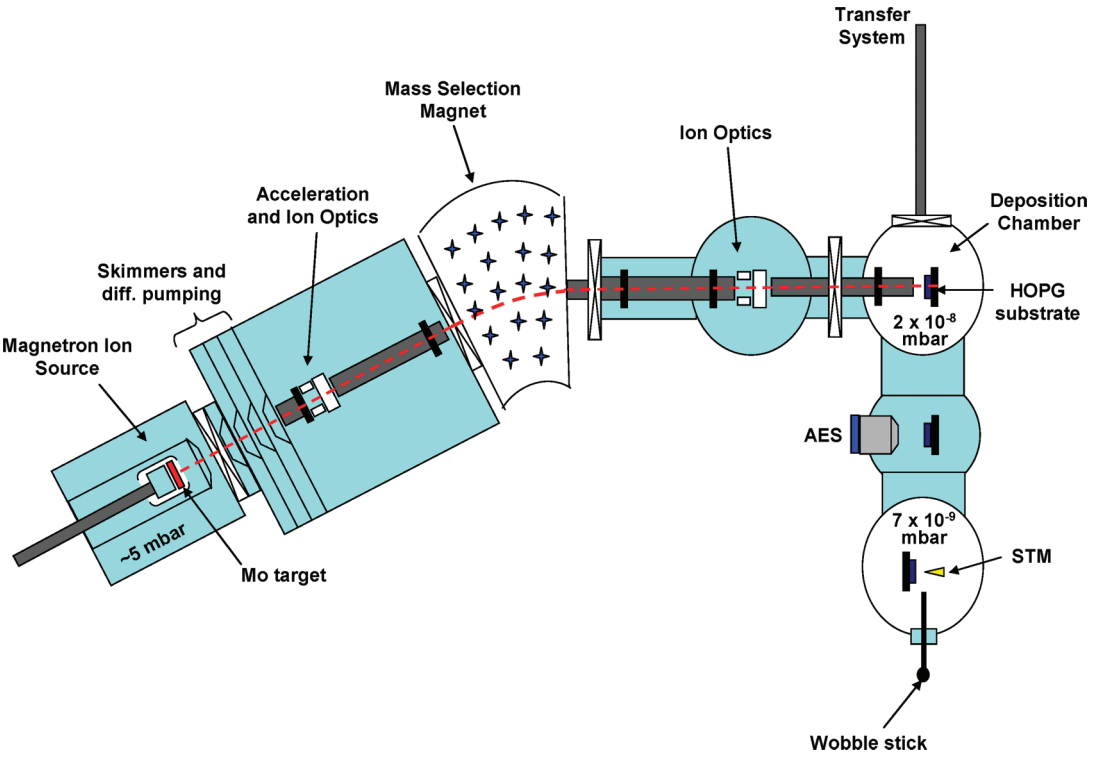

Figure 1. Schematic of our apparatus used for cluster deposition and *in situ* surface analysis.

trapped by high surface energy sites such as step-edges and other defects or until they nucleate to form larger aggregates. Since clusters on terraces can aggregate without constraint, they tend to grow larger than those on the step-edges.[71]

Despite the prevalence of metal cluster studies utilizing HOPG surfaces, there have been relatively few regarding metal oxide clusters deposited on HOPG.[102−105] This is surprising considering their importance in catalysis and other technological applications.[106] Furthermore, of those studies which have been conducted, the metal oxide clusters have usually been deposited either from solution[107] or by oxidation of deposited metal clusters.[108,109]

In the present study, we have investigated the chemical composition and surface morphologies of the size-selected, molybdenum and molybdenum oxide clusters, $Mo_{100\pm2.5}$ and $(MoO_3)_{67\pm1.5}$. Both species are soft-landed as cluster anions onto (conductive) HOPG surfaces, where they lose their charge and become neutral clusters. These particular cluster sizes were chosen because they have nearly equal masses and thus could be soft-landed with the same low kinetic energies. By using this approach, we were able to compare and contrast the different surface morphologies of two chemically distinct types of clusters on a common substrate. The overarching objective of this work was to compare how cluster composition and coverage regulate cluster surface morphology following deposition on HOPG.

EXPERIMENTAL SECTION

A schematic of our apparatus is presented in Figure 1. Molybdenum and molybdenum oxide cluster anions were produced using a magnetron sputter source[84] by mounting a molybdenum metal target in front of a permanent magnet, creating a cylindrical magnetic field. A mixture of helium and argon, typically 4:1 ratio of partial pressures and total pressure of ∼5 mbar, was injected into the ion source with the Mo target held at an applied voltage of −500 V. Argon ions created within the magnet field sputtered the molybdenum metal target, generating a plume of metal ions in the gas phase. Helium was used to both cool and transport the ions through the ion optics and mass selection magnet. To produce molybdenum oxide clusters, an additional 5−6% (partial pressure percentage) oxygen gas was added to the source. This amount of oxygen was well in excess of what is required to create fully oxidized molybdenum clusters (i.e., MoO_3). We verified this by varying the amount of oxygen added to the cluster source and then analyzing the chemical composition of these clusters by XPS. Incompletely oxidized molybdenum clusters created in the sputter source could be identified by the existence of significant (>5%) Mo(IV) in the XPS of the air-exposed samples, consistent with the behavior of purely metallic molybdenum clusters. Results from these XPS studies revealed that a partial pressure of ≈5% oxygen in the sputter system was more than sufficient to create molybdenum oxide clusters that exhibited <5% Mo(IV) after air exposure. This was taken as evidence that the as deposited molybdenum clusters created under these conditions were fully oxidized.

After being extracted from the source, the cluster anions were accelerated to 450 V and transported through a series of differential pumping stages and ion optics (see Figure 1). Mass selection was accomplished by passing the ion beam through a 25° sector magnet with a resolution of $m/\Delta m$ = 20. The performance of the magnet as a function of the magnetic field and beam energy was determined by using the mass spectrum of gold clusters as a reference. By adjusting the magnet field and the beam voltage appropriately, we were able to use the magnet to pass mass-selected $Mo_{100\pm2.5}^-$ and $(MoO_3)_{67\pm1.5}^-$ cluster anions downstream and into the next stage of the apparatus. The

dx.doi.org/10.1021/jp202165u |J. Phys. Chem. C XXXX, XXX, 000–000

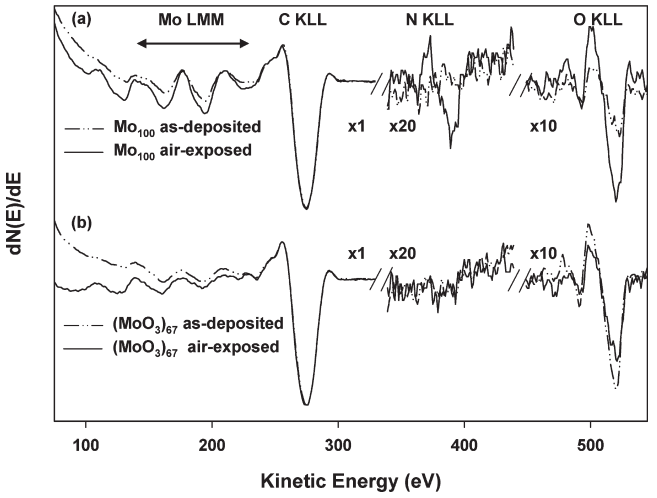

Figure 2. AE spectra of (a)$Mo_{100\pm2.5}$ and (b)$(MoO_3)_{67\pm1.5}$ clusters, both as-deposited (dashed line) and after air-exposure (solid line). Based on STM and AFM analysis, these spectra correspond to high coverages (>1 ML) of deposited clusters. The Auger transitions have been labeled, all spectra have been normalized to the height of the C KLL peak at 271 eV, and smaller features have been scaled as indicated.

mass distribution of our deposited clusters is determined by the resolution of the mass spectrometer, working with the assumption that the molybdenum oxide clusters are fully oxidized. The source conditions (e.g., the He/Ar ratio, total pressure, head/source distance, aperture potentials) were also optimized to maximize the intensity of the mass-selected clusters.

Once the cluster anions had been mass-selected, they were refocused and collimated by a series of ion optics before reaching the deposition chamber. The size-selected cluster anions were then decelerated to the desired deposition energy before landing on the HOPG substrate by biasing the target to the appropriate negative voltage. In the present study, the $Mo_{100\pm2.5}^-$ and $(MoO_3)_{67\pm1.5}^-$ anions were decelerated to kinetic energies of less than 0.1 eV per atom (well below the pinning threshold of ~10 eV/atom[90]) and thus soft-landed onto the HOPG surface. The pressure during cluster deposition was typically $\sim10^{-8}$ mbar.

The chemical composition of the deposited clusters was analyzed *in situ* using Auger electron spectroscopy (AES) and *ex situ* using X-ray photoelectron spectroscopy (XPS). AE spectra were acquired using an incident electron beam of 3 keV, and Auger electrons were analyzed using a double-pass CMA (DESA 100, STAIB Instruments, Inc.).[110] For XPS analysis, deposited cluster samples were removed from the deposition chamber and placed in a PHI 5400 XPS system and analyzed using Mg Kα X-rays (1253.6 eV). Ejected photoelectrons were measured with a precision high-energy electron analyzer operating at a constant pass-energy of 22.36 eV and a scan rate of 0.125 eV/step for the Mo(3d) spectral envelope (224−244 eV). Spectra were referenced to the C(1s) graphite peak (284.5 eV).[111] XP spectra were processed with commercially available software (CasaXPS) using mixed Gaussian (70%)/Lorentzian (30%) peaks with fixed Mo-$(3d_{5/2})$ peak positions at 232.3 ± 0.5 eV for Mo(VI) and 229.3 ± 0.5 eV for Mo(IV) and with a spin−orbit splitting of 3.13 eV for both oxidation states.[111]

To characterize the surface morphologies of deposited $Mo_{100\pm2.5}$ and $(MoO_3)_{67\pm1.5}$ clusters as a function of their surface coverage, a combination of *in situ* scanning tunneling microscopy (STM) and *ex situ* atomic force microscopy (AFM) was used. For *in situ* STM imaging, the HOPG targets were internally transferred from the deposition chamber to an adjoining UHV chamber, which contained an STM (Omicron 1). Hand-cut Pt/Ir tips were used in constant current mode with a gap voltage of 0.7 V and a tunneling current of 0.1 nA. STM image processing was performed with freely available software, WSxM.[112] For *ex situ* AFM imaging, the substrate was removed from the vacuum chamber and adhered to an AFM sample plate using double-sided carbon tape. Images were acquired using a PicoSPM LE AFM (Agilent Technologies) operated in magnetic tapping mode using Co−Cr tips obtained from MikroMasch (NSC18). All image rendering and height measurements were performed with commercially available software from Agilent Technologies.

RESULTS

Chemical Characterization of Deposited Clusters. From the *in situ* Auger spectra of as-deposited and air-exposed $Mo_{100\pm2.5}$ (Figure 2a) and $(MoO_3)_{67\pm1.5}$ clusters (Figure 2b), the chemical composition of the clusters was determined. In each spectrum, the C KLL peak at 271 eV associated with the HOPG substrate is the dominant feature. For the as-deposited $Mo_{100\pm2.5}$ clusters (Figure 2a, dashed line), molybdenum peaks along with a small peak associated with oxygen can be seen at 186 and 503 eV, respectively. When the $Mo_{100\pm2.5}$ clusters were air-exposed (Figure 2a, solid line), the oxygen peak increases in intensity, and there is a small but measurable nitrogen signal present at 379 eV, consistent with the production of predominantly metallic clusters that, upon air exposure, react with ambient oxygen and nitrogen. By contrast, *in situ* analysis of deposited $(MoO_3)_{67\pm1.5}$ clusters (Figure 2b, dashed line) exhibited significantly larger oxygen AES signals than the $Mo_{100\pm2.5}$ clusters, consistent with the deposition of metal oxide clusters. This assertion is also supported by the lack of a measurable change in the AE spectrum when as-deposited $(MoO_3)_{67\pm1.5}$ clusters were air exposed (Figure 2b, solid line).

Ex situ XPS analyses of air-exposed $Mo_{100\pm2.5}$ and $(MoO_3)_{67\pm1.5}$ clusters are shown in Figure 3. The Mo(3d) spectral envelope associated with deposited $(MoO_3)_{67\pm1.5}$ clusters reveals that the vast majority (>95%) of the molybdenum atoms are in the fully oxidized Mo(VI) state with a $Mo(3d_{5/2})$ peak centered at 232 eV, consistent with the production and deposition of MoO_3. In contrast for the air-exposed $Mo_{100\pm2.5}$ clusters, deconvolution of the Mo(3d) spectral envelope reveals nearly equal quantities of Mo(VI) and Mo(IV) species with $Mo(3d_{5/2})$ peaks at 232 and 229 eV, respectively. This is evidence for incomplete oxidation of the metallic molybdenum clusters upon air exposure. Taken in conjunction with the AES data, it is likely that the Mo(IV) peak is a result of some combination of MoO_2, oxynitride, or nitride species.

Surface Morphology of Deposited Clusters. *a. Metal Clusters.* Figure 4 shows both *ex situ* AFM (Figure 4a−d) and *in situ* STM (Figure 4e−g) images acquired of $Mo_{100\pm2.5}$ clusters soft-landed onto HOPG substrates, as a function of increasing coverage (i.e., increasing from (a) to (d) and from (e) to (g)). Both AFM and STM images clearly illustrate our ability to control the coverage of clusters on surfaces by varying exposure time or beam current. An estimate of the surface coverage was determined by first calculating the total ion dose, based on the ion current of the cluster beam and the duration of the deposition, assuming unity sticking probability. In addition, the

dx.doi.org/10.1021/jp202165u |J. Phys. Chem. C XXXX, XXX, 000–000

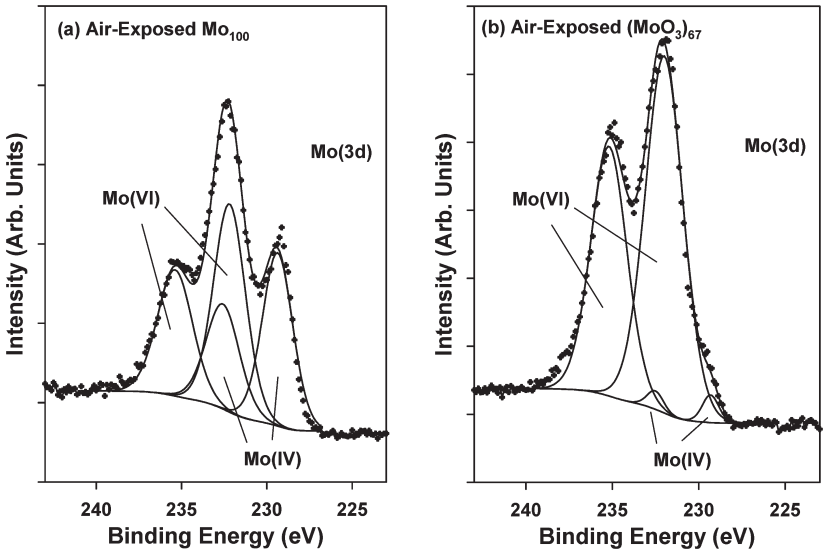

Figure 3. XP spectral envelopes of the Mo(3d) region for high-coverages of (a) $Mo_{100\pm2.5}$ and (b) $(MoO_3)_{67\pm1.5}$ clusters after air exposure. Component peaks for the Mo(IV) and Mo(VI) species are labeled.

diameter and thus the 2-dimensional footprint of both the metal and metal oxide clusters were calculated assuming spherical-shaped clusters with densities equal to the corresponding bulk materials. The values thus calculated were also qualitatively consistent with coverages determined from AFM and STM images. In this way, we determined that the low coverage regime corresponded to a cluster coverage of 0.01−0.2 ML, the medium coverage regime to be 0.2−0.8 ML, and the high coverage regime to be 2−5 ML.

At relatively low coverages (0.01−0.1 ML; see Figure 4a,e), clusters are observed to attach preferentially to step-edges. The heights for clusters residing along step-edges were measured by line scans, as shown in Figure 5a,b. However, as the coverage of deposited clusters increased (0.2−0.8 ML), the STM images became "streaky" (see Figure 4f). Nevertheless, using *ex situ* AFM imaging, we were able to image air-exposed $Mo_{100\pm2.5}$ clusters in this coverage regime, as shown in Figure 4b,c. In these images, clusters are observed to saturate the step-edges and begin to fill the terraces as coverage increases. In Figure 6, we compare the height of clusters arranged along step-edges (hashed bars) with those on terraces (solid bars). As the coverage continues to increase to ≥1 ML (2−5 ML), both AFM and STM images (Figure 4d,g) show that the metal clusters form overlayers composed of what appear to be individual clusters on the surface. Interestingly, at these high coverages, the image streaking that was observed at intermediate coverages was absent in the STM images.

b. Metal Oxide Clusters. Representative *in situ* STM micrographs of $(MoO_3)_{67\pm1.5}$ clusters deposited on HOPG are shown in Figure 7a−c as a function of increasing coverage (i.e., increasing from (a) to (c)). Figure 7a shows an STM image obtained at low coverage (0.01−0.1 ML) of deposited clusters, where the clusters are randomly distributed over the surface with no evidence of preferential step-edge nucleation. In Figure 7b, the $(MoO_3)_{67\pm1.5}$ cluster coverage has been increased, and the clusters continue to be stochastically distributed on the HOPG substrate. Moreover, there is no evidence of image streaking induced by the STM tip moving the adsorbed clusters in contrast to the behavior of metal clusters at comparable coverages (compare Figures 4f and 7b). At still higher coverages (2−5 ML; see Figure 7c), the $(MoO_3)_{67\pm1.5}$ clusters form what appears to be a loosely packed overlayer on the surface. At these high coverages, repeated STM imaging of the same area tended to "sweep" away clusters to reveal the underlying HOPG substrate. This is shown in Figure 8 at three successive scans of the same area. This sweeping of deposited clusters was a different phenomenon than the streaking observed in STM images of $Mo_{100\pm2.5}$ (see Figure 4f).

DISCUSSION

Here, we compare and contrast the morphologies of deposited $Mo_{100\pm2.5}$ and $(MoO_3)_{67\pm1.5}$ clusters as a function of surface coverage.

a. Low Cluster Coverages (0.01−0.1 ML). STM and AFM images of deposited $Mo_{100\pm2.5}$ clusters at low coverage (Figure 4a,e), both show that the metal clusters nucleate at the step-edges but not on the terraces. This is particularly apparent in the AFM image shown in Figure 4a, where a large number of individual clusters are observed along the step-edges, while the terraces remain empty. These observations are consistent with previous studies which have shown that the mobility of metal clusters on HOPG surfaces is high due to the relatively weak adsorbate−substrate interactions.[71,85,86,91] Consequently, the metal clusters diffuse freely upon deposition until they become "trapped" at the under-coordinated sites that exist at step-edges. It should also be noted that our observation of the behavior of the $Mo_{100\pm2.5}$ clusters is consistent with that of other metal clusters soft-landed on HOPG substrates[71,85,86,91] and also is consistent with our chemical characterization of the as-deposited clusters being predominantly metallic.

By contrast, $(MoO_3)_{67\pm1.5}$ metal oxide clusters behave differently at low coverages. STM images (see Figure 7a,b) show random distributions of deposited metal oxide clusters and an absence of preferential binding at step-edges. These results are consistent with the behavior of clusters which are relatively immobile on the surface, indicating that there is a significantly greater interaction between deposited metal oxide clusters and the HOPG substrate compared to metal clusters and HOPG.

dx.doi.org/10.1021/jp202165u |*J. Phys. Chem. C* XXXX, XXX, 000–000

The nucleation of metal clusters at the step-edges also allowed us to measure variations in their heights. Results from this analysis (see the line scan in Figure 5b) show that clusters arranged along the step-edge are uniform in size, with heights of 4.0 ± 1.0 nm. Since these structures appear to be individual clusters, this result confirms that sizes of mass-selected clusters deposited on the substrate are consistent.

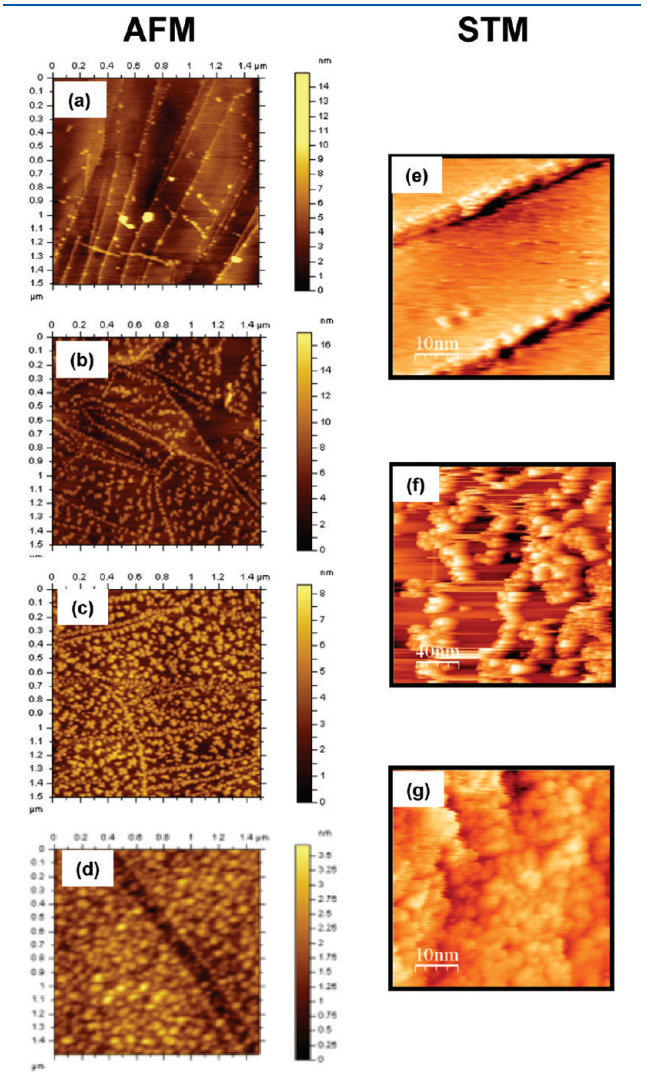

Figure 4. Deposited $Mo_{100\pm2.5}$ clusters on HOPG imaged by *ex situ* AFM (a−d) and *in situ* STM (e−g), shown as a function of increasing coverage (i.e., coverage increasing from (a) to (d) and from (e) to (g)).

Another important point is that the *ex situ* AFM and *in situ* STM images of deposited metal clusters in this low coverage regime are entirely consistent with one another despite the fact that the metal clusters oxidize when they are exposed to air (see Figure 3). For example, a comparison of Figures 4a and 4e reveals that in both AFM and STM images clusters are observed predominantly at the step-edge. This suggests that the morphologies of the deposited metal clusters are preserved upon air exposure, allowing us to use *ex situ* AFM to complement STM data. Furthermore, AFM is able to scan larger areas on the substrate compared to STM and therefore allows for more meaningful statistical analysis of the deposited clusters (i.e., a comparison of size distributions on step-edges versus on terraces).

b. Intermediate Cluster Coverages (0.2−0.8 ML). At increased coverage of $Mo_{100\pm2.5}$ clusters, the density of adsorbed metal clusters at the step-edge also increases until a local saturation coverage is reached. At that point, deposited metal clusters start to appear on the terraces (see the AFM image in Figure 4b). A combination of height analysis (Figure 6c) and 3-dimensional rendering (Figure 6b) of the *ex situ* AFM images reveals that the size and shape of adsorbates on the terraces differs from those at the step-edges; the average cluster height on the terrace is 5.9 ± 0.8 nm, while that of those on the step-edges is 4.0 ± 1.0 nm. Furthermore, the adsorbed structures observed on the terraces by AFM have larger 2-dimensional footprints and are more irregular in size and shape, consistent with the presence of aggregates composed of several metal clusters. Thus, it appears that metal cluster aggregation predominates on the terraces, while at the step-edges greater absorption energies immobilizes these same clusters and limits their aggregation. In contrast to the *ex situ* AFM images, *in situ* STM images acquired at similar (intermediate) coverages were often streaky (see Figure 4f), consistent with metal cluster mobility on the terraces. Thus, when compared to the *ex situ* AFM images taken at comparable coverages, it appears that partial oxidation of the deposited clusters upon air exposure also helps to immobilize them, consistent with the difference in behavior of $Mo_{100\pm2.5}$ and $(MoO_3)_{67\pm1.5}$ clusters observed *in situ* by STM. In contrast to the behavior of metal clusters in this coverage regime, deposited $(MoO_3)_{67\pm1.5}$ clusters did not lead to image streaking and remained randomly distributed on the surface, again suggesting stronger substrate interactions of metal oxide clusters compared to those of metal clusters.

c. Monolayer Cluster Coverages (2−5 ML). From both STM and AFM images, higher coverages (≥1 ML) of both $Mo_{100\pm2.5}$ and $(MoO_3)_{67\pm1.5}$ clusters resulted in the formation of densely packed arrays of clusters (see Figures 4d,g and 7c), where there is

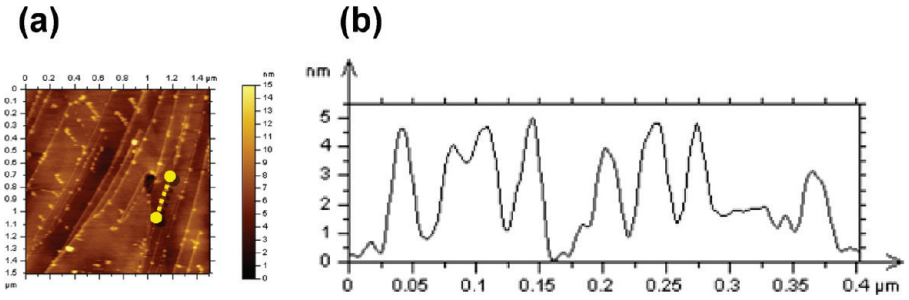

Figure 5. (a) AFM image of a low coverage of deposited $Mo_{100\pm2.5}$ clusters on HOPG after air exposure. (b) A line scan of the deposited clusters along the dotted line shown in (a).

dx.doi.org/10.1021/jp202165u |*J. Phys. Chem. C* XXXX, XXX, 000–000

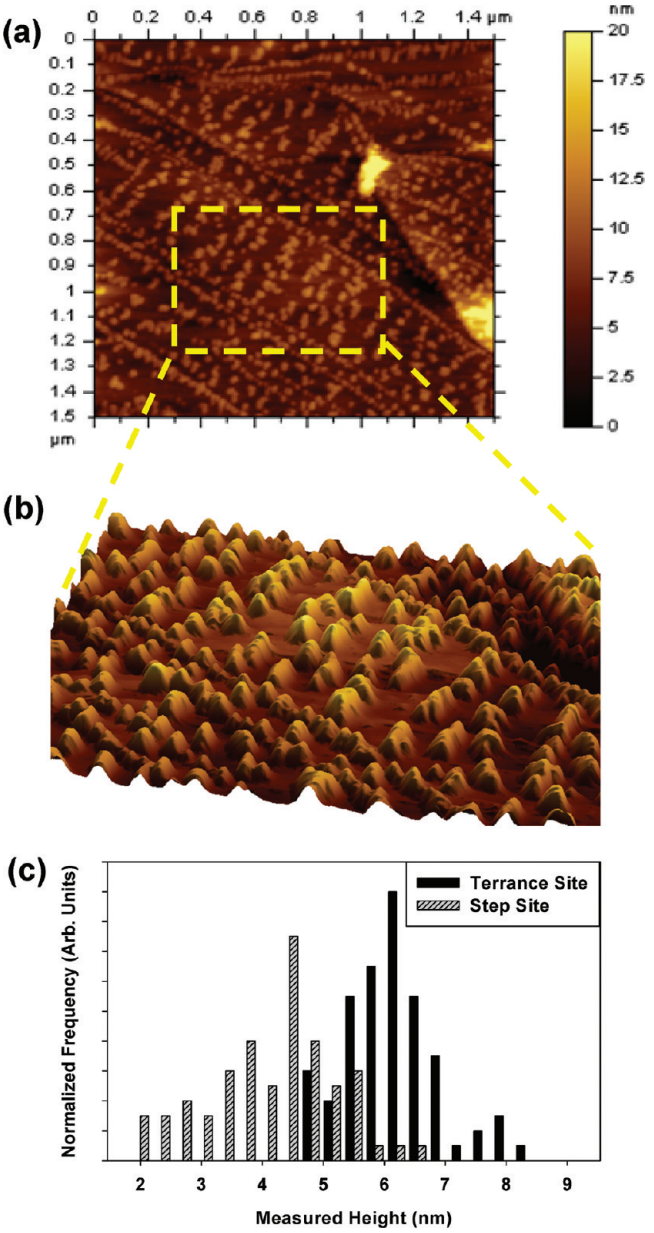

Figure 6. (a) AFM image of an intermediate coverage of deposited $Mo_{100\pm2.5}$ clusters on HOPG after air exposure, showing the presence of clusters on the step-edge and the terrace. (b) Three-dimensional rendering of the boxed region shown in (a), illustrating the presence of different sized features on the step-edges and the terraces. (c) Frequency-normalized histogram of cluster heights measured by AFM for $Mo_{100\pm2.5}$ clusters adsorbed on step-edges (hatched) and on terraces (filled).

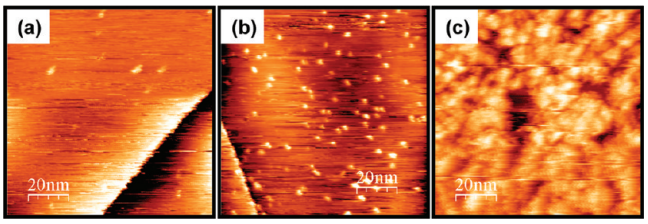

Figure 7. *In situ* STM images of $(MoO_3)_{67\pm1.5}$ clusters deposited on HOPG shown as a function of increasing coverage from (a) to (c).

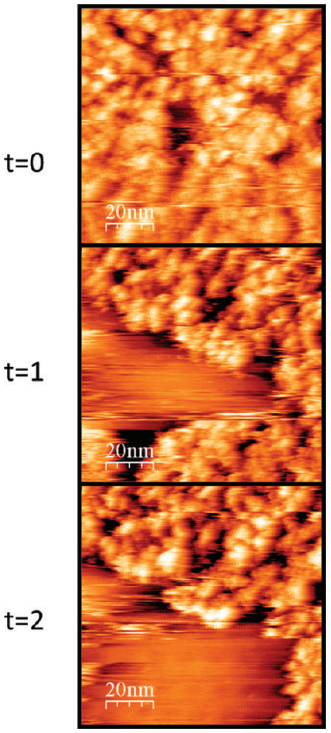

Figure 8. Change in the surface when $(MoO_3)_{67\pm1.5}$ clusters deposited on HOPG at high coverage are imaged repeatedly by a STM tip. Detailed analysis of the flat and featureless regions, uncovered with repeated sweeping, revealed the bare underlying HOPG substrate.

no visual evidence of the underlying HOPG substrate. Furthermore, the STM images resemble "grapelike" structures present on the surface, consistent with expectations for metal clusters deposited on surfaces. Interestingly, the stability of the deposited $Mo_{100\pm2.5}$ and $(MoO_3)_{67\pm1.5}$ clusters toward tip-induced displacement is reversed compared to the situation at lower coverages. At high coverages, the $Mo_{100\pm2.5}$ clusters were stable toward repeated STM imaging, while at high coverage $(MoO_3)_{67\pm1.5}$ clusters could be displaced by the STM tip to create vacant regions that revealed the underlying HOPG substrate (see Figure 8). As noted previously in the Results section, this behavior was distinct from the streaking observed with lower coverages of deposited $Mo_{100\pm2.5}$ clusters, which was, in fact, a consequence of cluster mobility.

The origin of the differences between the stabilities of $Mo_{100\pm2.5}$ and $(MoO_3)_{67\pm1.5}$ clusters toward tip-induced displacement at these higher coverages is unclear, but two possibilities seem most likely. One is that the observed differences are a reflection of fundamental changes to the distance (and thus the forces) between the STM tip and the adsorbed clusters due to changes in the tunneling characteristics. Another possibility is the oxide clusters are less strongly bound at higher coverages, and as a result the force between the STM tip and the clusters is now sufficient to displace them, while the increased stability of the metal clusters at higher coverages may be a consequence of their close packed arrangement, and the potential that metal−metal bonding between adjacent clusters could stabilize the adlayer.

d. Other Phenomena. Additional phenomena were occasionally observed with the STM while searching for deposited clusters. Figure 9a,b shows examples of a structure reminiscent

dx.doi.org/10.1021/jp202165u |*J. Phys. Chem. C* XXXX, XXX, 000–000

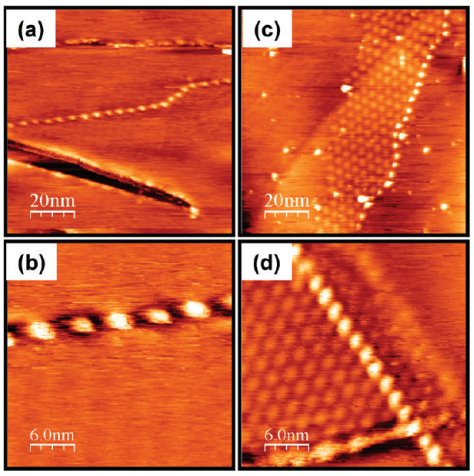

Figure 9. STM images of a grain boundary are shown in (a) and (b). Examples of Moiré patterns observed upon cluster deposition and in proximity to grain boundaries are shown in (c) and (d).

of an ordered array of deposited clusters at a step-edge. However, upon closer inspection it became clear that the structure is not, in fact, an array of clusters. The height of the surface is the same on both sides of the feature, inconsistent with the presence of a step-edge. Furthermore, the structure is quite regular over long distances and there is an alternating pattern of light and dark spots (see Figure 9b). On the basis of previous studies, we have concluded that this pattern is, in fact, the structure of a grain boundary on the HOPG surface caused by crystallographic defects characteristic of zone transitions between two graphite layers of different orientations.[94] Although these features were rare among our many surveys, their presence can cause confusion and highlight the need for rigor in identifying adsorbed clusters.

Another structure that we observed was the Moiré pattern (Figure 9c,d). This feature is the result of a rotational displacement of the uppermost surface layer of HOPG, which gives rise to an electronic interference pattern with the underlying layers of graphite.[95−98] Previous studies have shown that these patterns can occur naturally on the HOPG surface[99] but are more often caused by exposure to intercalating solvents[94] or metal clusters[100,101] which insert between the graphene layers and physically displace the uppermost surface layer of graphite. Interestingly, we observed Moiré patterns on HOPG only after cluster deposition. In fact, we have on many occasions observed clusters situated within the Moiré pattern itself, as shown in Figure 9c. Furthermore, these patterns were often bordered on at least one side by the aforementioned grain boundary (see Figure 9d). These observations suggest that deposited clusters can impact the local density of electronic states in the HOPG substrate.

CONCLUSIONS

Metal and metal oxide clusters of molybdenum behaved differently when they were soft-landed on HOPG with the same incident kinetic energy. At low coverages, the metal clusters are highly mobile on the surface and nucleate exclusively at under-coordinated step-edge sites, while the metal oxide clusters are comparatively immobile, presumably a consequence of stronger cluster−substrate interactions. Once step-edge sites had become saturated, metal clusters formed aggregates on the terraces. In contrast to the situation at lower coverages, monolayer coverages of deposited metal clusters were more stable toward tip-induced displacement than were the metal oxide clusters. Results from the present investigation illustrate how the surface morphologies of adsorbed clusters are influenced by their chemical composition, their interactions with the substrate, and their coverage.

AUTHOR INFORMATION

Corresponding Author

*E-mail: kbowen@jhu.edu (K.H.B.), howardf@jhu.edu (D.H.F.), gerd.gantefoer@uni-konstanz.de (G.G.).

Present Addresses

†Physics Department, University of Konstanz, Konstanz, Germany.

ACKNOWLEDGMENT

This work was supported by the Division of Materials Science and Engineering, Basic Energy Sciences, U.S. Department of Energy, under Grant DE-FG02-09ER46558. The authors also thank the JHU Materials Sciences Surface Analysis Laboratory for XPS analysis. K.A.W. also acknowledges the JHU Department of Chemistry for the Rudolf Sonneborn Fellowship.

REFERENCES

(1) Castleman, A. W.; Bowen, K. H. *J. Phys. Chem.* **1996**, *100*, 12911.
(2) Basir, Y. J.; Anderson, S. L. *Int. J. Mass Spectrom.* **1999**, *185/186/187*, 603.
(3) Armentrout, P. B. *Annu. Rev. Phys. Chem.* **2001**, *52*, 523.
(4) Xie, Y.; Dong, F.; Heinbuch, S.; Rocca, J. J.; Bernstein, E. R. *Phys. Chem. Chem. Phys.* **2010**, *12*, 947.
(5) Popolan, D. M.; Nössler, M.; Mitrić, R.; Bernhardt, T. M.; Bonačić-Koutecký, V. *J. Phys. Chem. A* **2011**, *115*, 951.
(6) Hanmura, T.; Ichihashi, M.; Watanabe, Y.; Isomura, N.; Kondow, T. *J. Phys. Chem. A* **2007**, *111*, 422.
(7) Vajda, S.; Wolf, S.; Leisner, T.; Busolt, U.; Wöste, L. H.; Wales, D. J. *J. Chem. Phys.* **1997**, *107*, 3492.
(8) Riley, S. J. *Z. Phys. D* **1989**, *12*, 537.
(9) Morse, M. D.; Geusic, M. E.; Heath, J. R.; Smalley, R. E. *J. Chem. Phys.* **1985**, *83*, 2293.
(10) Schlangen, M.; Schwarz, H. *Chem. Commun.* **2010**, *46*, 1878.
(11) Whetten, R. L.; Homer, M. L.; Li, X.; Livingston, F. E., St.; John, P. M.; Becker, R. D. *Ber. Bunsen-Ges. Phys. Chem.* **1992**, *96*, 1120.
(12) Bloomfield, L. A.; Bucher, J. P.; Douglass, D. C. Magnetic structure of clusters. In *On Clusters and Clustering, From Atoms to Fractals*; Reynolds, P. J., Ed.; Elsevier: Amsterdam, 1993.
(13) de Heer, W. A. *Rev. Mod. Phys.* **1993**, *65*, 611.
(14) Knickelbein, M. B. *J. Chem. Phys.* **2006**, *125*, 044308.
(15) Kaldor, A.; Cox, D. M.; Zakin, M. R. Molecular surface chemistry: Reactions of gas-phase metal clusters. In *Evolution of Size Effects in Chemical Dynamics*; Prigogine, I., Rice, S. A., Eds.; Wiley: New York, 1988; pp 211−261.
(16) Claridge, S. A.; Castleman, A. W.; Khanna, S. N.; Murray, C. B.; Sen, A.; Weiss, P. S. *ACS Nano* **2009**, *3*, 244.
(17) Horn, J. M.; Song, Z.; Potapenko, D. V.; Hrbek, J.; White, M. G. *J. Phys. Chem. B* **2004**, *109*, 44.
(18) Bondarchuk, O.; Huang, X.; Kim, J.; Kay, B. D.; Wang, L.-S.; White, J. M.; Dohnálek, Z. *Angew. Chem., Int. Ed.* **2006**, *45*, 4786.
(19) Potapenko, D. V.; Horn, J. M.; Beuhler, R. J.; Song, Z.; White, M. G. *Surf. Sci.* **2005**, *574*, 244.
(20) Winans, R. E.; Vajda, S.; Lee, B.; Riley, S. J.; Seifert, S.; Tikhonov, G. Y.; Tomczyk, N. A. *J. Phys. Chem. B* **2004**, *108*, 18105.
(21) Lee, B.; Seifert, S.; Riley, S. J.; Tikhonov, G.; Tomczyk, N. A.; Vajda, S.; Winans, R. E. *J. Chem. Phys.* **2005**, *123*, 074701.

(22) Stegemann, B.; Bernhardt, T. M.; Kaiser, B.; Rademann, K. *Surf. Sci.* **2002**, *511*, 153.
(23) Bardotti, L.; Tournus, F.; Mélinon, P.; Pellarin, M.; Broyer, M. *Phys. Rev. B* **2011**, *83*, 035425.
(24) Kemper, P.; Kolmakov, A.; Tong, X.; Lilach, Y.; Benz, L.; Manard, M.; Metiu, H.; Buratto, S. K.; Bowers, M. T. *Int. J. Mass Spectrom.* **2006**, *254*, 202.
(25) Tong, X.; Benz, L.; Kemper, P.; Metiu, H.; Bowers, M. T.; Buratto, S. K. *J. Am. Chem. Soc.* **2005**, *127*, 13516.
(26) Cuppens, J.; Romero, C. P.; Lievens, P.; Van Bael, M. J. *Phys. Rev. B* **2010**, *81*, 064517.
(27) Yasumatsu, H.; Hayakawa, T.; Koizumi, S. I.; Kondow, T. *Trans. Mater. Res. Soc. Jpn.* **2002**, *27*, 209.
(28) Lei, Y.; Mehmood, F.; Lee, S.; Greeley, J.; Lee, B.; Seifert, S.; Winans, R. E.; Elam, J. W.; Meyer, R. J.; Redfern, P. C.; Teschner, D.; Schlogl, R.; Pellin, M. J.; Curtiss, L. A.; Vajda, S. *Science* **2010**, *328*, 224.
(29) Lightstone, J. M.; Patterson, M. J.; Liu, P.; Lofaro, J. C.; White, M. G. *J. Phys. Chem. C* **2008**, *112*, 11495.
(30) Lee, S.; Fan, C.; Wu, T.; Anderson, S. L. *J. Am. Chem. Soc.* **2004**, *126*, 5682.
(31) Kaden, W. E.; Wu, T.; Kunkel, W. A.; Anderson, S. L. *Science* **2009**, *326*, 826.
(32) Lee, S.; Fan, C.; Wu, T.; Anderson, S. L. *J. Phys. Chem. B* **2005**, *109*, 11340.
(33) Aizawa, M.; Lee, S.; Anderson, S. L. *Surf. Sci.* **2003**, *542*, 253.
(34) Aizawa, M.; Lee, S.; Anderson, S. L. *J. Chem. Phys.* **2002**, *117*, 5001.
(35) Fan, C.; Wu, T.; Kaden, W. E.; Anderson, S. L. *Surf. Sci.* **2006**, *600*, 461.
(36) Vajda, S.; Winans, R.; Elam, J.; Lee, B.; Pellin, M.; Seifert, S.; Tikhonov, G.; Tomczyk, N. *Top. Catal.* **2006**, *39*, 161.
(37) Lee, S.; Lee, B.; Mehmood, F.; Seifert, S.; Libera, J. A.; Elam, J. W.; Greeley, J.; Zapol, P.; Curtiss, L. A.; Pellin, M. J.; Stair, P. C.; Winans, R. E.; Vajda, S. *J. Phys. Chem. C* **2010**, *114*, 10342.
(38) Eberhardt, W.; Fayet, P.; Cox, D. M.; Fu, Z.; Kaldor, A.; Sherwood, R.; Sondericker, D. *Phys. Rev. Lett.* **1990**, *64*, 780.
(39) Roy, H. V.; Fayet, P.; Patthey, F.; Schneider, W. D.; Delley, B.; Massobrio, C. *Phys. Rev. B* **1994**, *49*, 5611.
(40) Messerli, S.; Schintke, S.; Morgenstern, K.; Sanchez, A.; Heiz, U.; Schneider, W.-D. *Surf. Sci.* **2000**, *465*, 331.
(41) Landman, U.; Yoon, B.; Zhang, C.; Heiz, U.; Arenz, M. *Top. Catal.* **2007**, *44*, 145.
(42) Kunz, S.; Hartl, K.; Nesselberger, M.; Schweinberger, F. F.; Kwon, G.; Hanzlik, M.; Mayrhofer, K. J. J.; Heiz, U.; Arenz, M. *Phys. Chem. Chem. Phys.* **2010**, *12*, 10288.
(43) Heiz, U.; Schneider, W.-D. *Crit. Rev. Solid State Mater. Sci.* **2001**, *26*, 251.
(44) Hagen, J.; Socaciu, L. D.; Elijazyfer, M.; Heiz, U.; Bernhardt, T. M.; Woste, L. *Phys. Chem. Chem. Phys.* **2002**, *4*, 1707.
(45) Arenz, M.; Landman, U.; Heiz, U. *ChemPhysChem* **2006**, *7*, 1871.
(46) Harding, C.; Habibpour, V.; Kunz, S.; Farnbacher, A. N.-S.; Heiz, U.; Yoon, B.; Landman, U. *J. Am. Chem. Soc.* **2008**, *131*, 538.
(47) Lim, D. C.; Dietsche, R.; Ganteför, G.; Kim, Y. D. *Appl. Surf. Sci.* **2009**, *256*, 1148.
(48) Lim, D. C.; Dietsche, R.; Ganteför, G.; Kim, Y. D. *Chem. Phys.* **2009**, *359*, 161.
(49) Lim, D. C.; Dietsche, R.; Ganteför, G.; Kim, Y. D. *Chem. Phys. Lett.* **2008**, *457*, 391.
(50) Lim, D. C.; Dietsche, R.; Bubek, M.; Ganteför, G.; Kim, Y. D. *ChemPhysChem* **2006**, *7*, 1909.
(51) Popok, V. N.; Campbell, E. E. B. *Rev. Adv. Mater. Sci.* **2006**, *11*, 19.
(52) Palmer, R. E.; Pratontep, S.; Boyen, H.-G. *Nature Mater.* **2003**, *2*, 443.
(53) Habrich, W. In *Metal Clusters at Surfaces*; Maiwess-Broer, K. H., Ed.; Springer: Berlin, 2000; p 107.
(54) Wegner, K.; Piseri, P.; Tafreshi, H. V.; Milani, P. *J. Phys. D: Appl. Phys.* **2006**, *39*, R439.
(55) Bernhardt, T. M.; Kaiser, B.; Rademann, K. *Phys. Chem. Chem. Phys.* **2002**, *4*, 1192.
(56) Bromann, K.; Felix, C.; Brune, H.; Harbich, W.; Monot, R.; Buttet, J.; Kern, K. *Science* **1996**, *274*, 956.
(57) Bettac, A.; Köller, L.; Rank, V.; Meiwes-Broer, K. H. *Surf. Sci.* **1998**, *402*−*404*, 475.
(58) Jonas, K. L.; Bettac, A.; Rank, V.; Meiwes-Broer, K. H. Scannng tunneling spectroscopy on silver clusters. In *Structure and Dynamics of Heterogeneous Systems: From Atoms, Molecules and Clusters in Complex Environment to Thin Films and Multilayers, International Symposium*; Entel, P., Wolf, D. E., Eds.; World Scientific Publishing Co. Pte. Ltd: Duisburg, Germany, 1999; p 59.
(59) Methling, R. P.; Senz, V.; Klinkenberg, E. D.; Diederich, T.; Tiggesbäumker, J.; Holzhüter, G.; Bansmann, J.; Meiwes-Broer, K. H. *Eur. Phys. J. D* **2001**, *16*, 173.
(60) Getzlaff, M.; Bansmann, J.; Bulut, F.; Gebhardt, R. K.; Kleibert, A.; Meiwes-Broer, K. H. *Appl. Phys. A: Mater. Sci. Process.* **2006**, *82*, 95.
(61) Jonas, K. L.; von Oeynhausen, V.; Bansmann, J.; Meiwes-Broer, K. H. *Appl. Phys. A: Mater. Sci. Process.* **2006**, *82*, 131.
(62) Meiwes-Broer, K. H. *Clusters at Surfaces: Electronic Properties and Magnetism*; Springer: Heidelberg, Germany, 2006.
(63) Kleibert, A.; Meiwes-Broer, K. H.; Bansmann, J. *Phys. Rev. B* **2009**, *79*, 125423.
(64) Barke, I.; Zheng, F.; Bockenhauer, S.; Sell, K.; Oeynhausen, V. v.; Meiwes-Broer, K. H.; Erwin, S. C.; Himpsel, F. J. *Phys. Rev. B* **2009**, *79*, 155301.
(65) Duffe, S.; Irawan, T.; Bieletzki, M.; Richter, T.; Sieben, B.; Yin, C.; von Issendorff, B.; Moseler, M.; Hövel, H. *Eur. Phys. J. D* **2007**, *45*, 401.
(66) Tong, X.; Benz, L.; Kemper, P.; Metiu, H.; Bowers, M. T.; Buratto, S. K. *J. Am. Chem. Soc.* **2005**, *127*, 13516.
(67) Tong, X.; Benz, L.; Chretien, S.; Kemper, P.; Kolmakov, A.; Metiu, H.; Bowers, M. T.; Buratto, S. K. *J. Chem. Phys.* **2005**, *123*, 204701.
(68) Kemper, P.; Kolmakov, A.; Tong, X.; Lilach, Y.; Benz, L.; Manard, M.; Metiu, H.; Buratto, S. K.; Bowers, M. T. *Int. J. Mass Spectrom.* **2006**, *254*, 202.
(69) Smith, R.; Nock, C.; Kenny, S. D.; Belbruno, J. J.; Di Vece, M.; Palomba, S.; Palmer, R. E. *Phys. Rev. B* **2006**, *73*, 125429.
(70) Yin, F.; Xirouchaki, C.; Guo, Q.; Palmer, R. E. *Adv. Mater.* **2005**, *17*, 731.
(71) Carroll, S. J.; Seeger, K.; Palmer, R. E. *Appl. Phys. Lett.* **1998**, *72*, 305.
(72) Carroll, S. J.; Hall, S. G.; Palmer, R. E.; Smith, R. *Phys. Rev. Lett.* **1998**, *81*, 3715.
(73) Gibilisco, S.; Di Vece, M.; Palomba, S.; Faraci, G.; Palmer, R. E. *J. Chem. Phys.* **2006**, *125*, 084704.
(74) Carroll, S. J.; et al. *J. Phys.: Condens. Matter* **1996**, *8*, L617.
(75) Pratontep, S.; Preece, P.; Xirouchaki, C.; Palmer, R. E.; Sanz-Navarro, C. F.; Kenny, S. D.; Smith, R. *Phys. Rev. Lett.* **2003**, *90*, 055503.
(76) Jester, S.-S.; Löffler, D.; Weis, P.; Böttcher, A.; Kappes, M. M. *Surf. Sci.* **2009**, *603*, 1863.
(77) Wortmann, B.; Mende, K.; Duffe, S.; Grönhagen, N.; von Issendorff, B.; Hövel, H. *Phys. Status Solidi B* **2010**, *247*, 1116.
(78) Dietsche, R.; Lim, D. C.; Bubek, M.; Lopez-Salido, I.; Ganteför, G.; Kim, Y. D. *Appl. Phys. A: Mater. Sci. Process.* **2008**, *90*, 395.
(79) Lim, D. C.; Hwang, C.-C.; Gantefor, G.; Kim, Y. D. *Phys. Chem. Chem. Phys.* **2010**, *12*, 15172.
(80) Lopez-Salido, I.; Bertram, N.; Lim, D. C.; Ganteför, G.; Kim, Y. D. *Bull. Korean Chem. Soc.* **2006**, *27*, 556.
(81) Löffler, D.; Weis, P.; Malik, S.; ttcher, A.; Kappes, M. M. *Phys. Rev. B* **2008**, *77*, 155405.
(82) Vučković, S.; Samela, J.; Nordlund, K.; Popok, V. N. *Eur. Phys. J. D* **2009**, *52*, 107.
(83) Seminara, L.; Convers, P.; Monot, R.; Harbich, W. *Eur. Phys. J. D* **2004**, *29*, 49.
(84) Lim, D. C.; Dietsche, R.; Bubek, M.; Ketterer, T.; Ganteför, G.; Kim, Y. D. *Chem. Phys. Lett.* **2007**, *439*, 364.
(85) Hayakawa, T.; Yasumatsu, H.; Kondow, T. *Eur. Phys. J. D* **2009**, *52*, 95.

(86) Busolt, U.; Cottancin, E.; Socaciu, L.; Röhr, H.; Leisner, T.; Wöste, L. *Eur. Phys. J. D* **2001**, *16*, 297.
(87) Kaiser, B.; Bernhardt, T. M.; Stegemann, B.; Opitz, J.; Rademann, K. *Phys. Rev. Lett.* **1999**, *83*, 2918.
(88) Kaiser, B.; Bernhardt, T. M.; Stegemann, B.; Opitz, J.; Rademann, K. *Nucl. Instrum. Methods Phys. Res., Sect. B* **1999**, *157*, 155.
(89) Kaiser, B.; Bernhardt, T. M.; Rademann, K. *Nucl. Instrum. Methods Phys. Res., Sect. B* **1997**, *125*, 223.
(90) Xirouchaki, C.; Palmer, R. E. *Vacuum* **2002**, *66*, 167.
(91) Bardotti, L.; Jensen, P.; Hoareau, A.; Treilleux, M.; Cabaud, B. *Phys. Rev. Lett.* **1995**, *74*, 4694.
(92) Mellita, C.; Sharon, F. *J. Phys.: Condens. Matter* **2005**, *17*, R995.
(93) Jensen, P. *Rev. Mod. Phys.* **1999**, *71*, 1695.
(94) Wang, Y.; Ye, Y.; Wu, K. *Surf. Sci.* **2006**, *600*, 729.
(95) Kuwabara, M.; Clarke, D. R.; Smith, D. A. *Appl. Phys. Lett.* **1990**, *56*, 2396.
(96) Xhie, J.; Sattler, K.; Ge, M.; Venkateswaran, N. *Phys. Rev. B* **1993**, *47*, 15835.
(97) Rong, Z. Y.; Kuiper, P. *Phys. Rev. B* **1993**, *48*, 17427.
(98) Osing, J.; Shvets, I. *V. Surf. Sci.* **1998**, *417*, 145.
(99) Zhang, J.-f.; Cao, G.-y. *Chin. J. Chem. Phys.* **2006**, *19*, 197.
(100) Xu, H.; Permana, H.; Lu, Y.; Ng, K. Y. S. *Surf. Sci.* **1995**, *325*, 285.
(101) Tanii, T.; Hara, K.; Ishibashi, K.; Ohta, K.; Ohdomari, I. *Appl. Surf. Sci.* **2000**, *162−163*, 662.
(102) Shyjumon, I.; Gopinadhan, M.; Helm, C. A.; Smirnov, B. M.; Hippler, R. *Thin Solid Films* **2006**, *500*, 41.
(103) Chen, Y. P.; Ding, K.; Yang, L.; Xie, B.; Song, F. Q.; Wan, J. G.; Wang, G. G.; Hana, M. *Appl. Phys. Lett.* **2008**, *92*, 173112.
(104) Tanaka, N.; Peng, D. L.; Sumiyama, K.; Hihara, T. *Thin Solid Films* **2008**, *516*, 1677.
(105) Price, S. P.; Tong, X.; Ridge, C.; Shapovalov, V.; Hu, Z.; Kemper, P.; Metiu, H.; Bowers, M. T.; Buratto, S. K. *Sur. Sci.* **2011**, *605*, 972.
(106) Chambers, S. A. *Surf. Sci. Rep.* **2000**, *39*, 105.
(107) Murray, B. J.; Li, Q.; Newberg, J. T.; Hemminger, J. C.; Penner, R. M. *Chem. Mater.* **2005**, *17*, 6611.
(108) Kadossov, E.; Funk, S.; Burghaus, U. *Catal. Lett.* **2008**, *120*, 179.
(109) Lim, D. C.; Lopez-Salido, I.; Dietsche, R.; Bubek, M.; Kim, Y. D. *Surf. Sci.* **2006**, *600*, 507.
(110) Davis, L. E.; MacDonald, N. C.; Palmberg, P. W.; Riach, G. *Handbook of Auger Electron Spectroscopy*; Physical Electronics Publishing: Eden Prairie, MN, 1978.
(111) Moulder, J. F.; Stickle, W. F.; Sobol, P. E.; Bomben, K. D. In *Handbook of X-ray Photoelectron Spectroscopy*; Chastain, J., King, R. C., Jr., Eds.; Physical Electronics Publishing: Eden Prairie, MN, 1995.
(112) Horcas, I.; Fernandez, R.; Gomez-Rodriguez, J. M.; Colchero, J.; Gomez-Herrero, J.; Baro, A. M. *Rev. Sci. Instrum.* **2007**, *78*, 013705.